Interaction of Poly(vinylidene fluoride) with Graphite Particles. 1. Surface Morphology of a Composite Film and Its Relation to Processing Parameters

Mikyong Yoo,[†] Curtis W. Frank,*[,†,‡] and Shoichiro Mori[§,||]

Department of Materials Science and Engineering and Department of Chemical Engineering, Stanford University, Stanford, California 94305, and Mitsubishi Chemical Corporation, Tsukuba Research Center, 8-3-1 Chuo, Ami, Inashiki, Ibaraki 300-03, Japan

Received October 9, 2002

In lithium ion battery composite anodes that are derived from graphite particles bound together by a polymeric binder of 5−7 wt %, it is well-known that the type and content of the binder influence the formation of a solid electrolyte interphase and the electrochemical behavior. However, the nature of the interaction between the graphite particles and binder has not been extensively studied. We describe here the interaction of poly(vinylidene fluoride) (PVDF) with graphite based on the characteristics of the precursor slurry and the surface chemistry and morphology of the final composite anodes. The slurry was characterized by dynamic viscosity measurements and the solid composite by atomic force microscopy, lateral force microscopy, electron probe X-ray microanalysis, and X-ray photoelectron spectroscopy. The final film properties correlate with the suspension viscosity, which varies over 6 orders of magnitude for eight different carbon samples. In the composite film, PVDF preferentially deposits on the edges and grain boundaries of the graphite particles with a maximum of 40% of the surface of graphite being covered by the polymer. We correlate an increase in the homogeneity of the PVDF distribution in the final composite film with an increase in the slurry viscosity and interpret this observation in terms of PVDF/graphite interaction.

Introduction

The lithium ion rechargeable battery has been developed commercially because of its improved safety and cycle life, along with an energy density that is similar to that of lithium metal batteries.[1] Operation is based on the concept of a rocking chair or shuttlecock, where lithium ions can reversibly intercalate and deintercalate between carbonaceous anodes and metal transition oxide cathodes. Charging occurs when lithium ions are injected into the anode, which consists predominantly of graphite particles bound by a polymeric binder such as poly(vinylidene fluoride) (PVDF).

One of the important characteristics of a lithium ion battery is its reversibility,[1] in that low reversibility of lithium ions exchanged between the two electrodes leads to an irreversible capacity. The irreversible capacity, which is determined by the quantity of lithium ions not reversed between the two electrodes during cycling, mainly arises due to the formation of a solid electrolyte interphase (SEI). It is well-known that the SEI results from decomposition of the electrolyte due to unwanted side reactions when the Li^+ ion intercalates.[2,3] Once formed, the SEI prevents the further co-intercalation of solvent into the graphite layers, which can lead to electrode destruction upon cycling.[3] The irreversible capacity may also exist due to kinetic effects that lead to a portion of the lithium being trapped.[4] Finally, the irreversible capacity has been found to depend on graphite particle size,[5] number of active sites,[6] type of heteroatoms,[7] nature of surface structural defects,[8] and binder composition.[9−11]

The polymeric binder, which is necessary to provide sufficient mechanical strength to the electrodes, can also undergo electrochemical reaction. Reactions of the binder with the Li^+ ion of lithiated carbon do not begin until temperatures above 300 °C, so a direct reaction is not considered to be important during processing and

* To whom correspondence should be addressed. E-mail: curt@chemeng.stanford.edu.

[†] Department of Materials Science and Engineering, Stanford University.

[‡] Department of Chemical Engineering, Stanford University.

[§] Mitsubishi Chemical Corporation.

[||] Currently at National Institute for Materials Science, 1-2-1 Sengen, Tsukuba, Ibaraki 305-0047, Japan.

(1) Flandrois, S.; Simon, B. *Carbon* **1999**, *37*, 165.

(2) Aurbach, D.; Daroux, M. L.; Faguy, P. W.; Yeager, E. *J. Electrochem. Soc.* **1987**, *134*, 1611.

(3) Fong, R.; Vonsacken, U.; Dahn, J. R. *J. Electrochem. Soc.* **1990**, *137*, 2009.

(4) Smart, M. C.; Ratnakumar, B. V.; Surampudi, S.; Wang, Y.; Zhang, X.; Greenbaum, S. G.; Hightower, A.; Ahn, C. C.; Fultz, B. *J. Electrochem. Soc.* **1999**, *146*, 3963.

(5) Zaghib, K.; Nadeau, G.; Kinoshita, K. *J. Electrochem. Soc.* **2000**, *147*, 2110.

(6) Tran, T.; Yebka, B.; Song, X.; Nazri, G.; Kinoshita, K.; Curtis, D. *J. Power Sources* **2000**, *85*, 269.

(7) Larcher, D.; Mudalige, C.; George, A. E.; Porter, V.; Gharghouri, M.; Dahn, J. R. *Solid State Ionics* **1999**, *122*, 71.

(8) Flandrois, S.; Guerin, K. *Mol. Cryst. Liq. Cryst.* **2000**, *340*, 493.

(9) Li, G. B.; Xue, R. J.; Chen, L. Q. *Solid State Ionics* **1996**, *90*, 221.

(10) Liu, W. F.; Huang, X. J.; Li, G. B.; Wang, Z. X.; Huang, H.; Lu, Z. H.; Xue, R. J.; Chen, L. Q. *J. Power Sources* **1997**, *68*, 344.

(11) Chusid, O.; Ely, Y. E.; Aurbach, D.; Babai, M.; Carmeli, Y. *J. Power Sources* **1993**, *43*, 47.

10.1021/cm0209970 CCC: $25.00
Published on Web 02/01/2003

Table 1. Manufacturer, Type of Carbon, Average Particle Size (μm), BET Surface Area (m^2/g), and Real Component of Complex Viscosity for Eight Carbon Materials That Were Used for Experiments[a]

	manufacturer	type of carbon	average particle size (μm)	BET surface area (m^2/g)	real component of complex viscosity (N·s/m^2, at 1 rad/s)
MPG-V2	Mitsubishi Chemical Co., Japan	synthetic graphite	18.4	2.8	1.96×10^{-1}
MBC-N	Mitsubishi Chemical Co., Japan	amorphous carbon	18.0	5.0	4.00×10^{-1}
MCMB	Oosaka Gas Chem., Japan	synthetic graphite	7.8	3.3	1.74×10^{2}
SFG44	Timcal Co. Ltd., Switzerland	synthetic graphite	22.0	5.0	9.57×10^{2}
SFG75	Timcal Co. Ltd., Switzerland	synthetic graphite	27.0	3.5	5.04×10^{3}
KS15	Timcal Co. Ltd., Switzerland	synthetic graphite	7.7	12.0	7.56×10^{3}
SFG15	Timcal Co. Ltd., Switzerland	synthetic graphite	8.1	8.8	1.12×10^{4}
KS6	Timcal Co. Ltd., Switzerland	synthetic graphite	3.3	20.0	2.96×10^{4}

[a] For the real component of complex viscosity, PVDF350 binder was used and the compositional mix of carbon particles:PVDF:solvent in slurries was 38:2:60 wt %.

normal operation, which are carried out at much lower temperature.[12] However, it is known that the details of the surface chemistry and the morphology of the carbon play important roles in SEI formation.[11,13] Moreover, it has been reported that up to 70% of the graphite surface was covered by the PVDF binder, even though the binder concentration was kept relatively low.[14] Thus, the binder does influence the electrochemical reaction between lithium ions and electrolyte that takes place at the carbon surface.

The influence of the binder on the irreversible capacity has been investigated by several researchers.[9−11,15−17] It has been shown that the reversibility decreased as the amount of the binder increased, with a binder concentration of 4−5 wt % being optimum.[11] The highest degree of reversible intercalation was obtained when PVDF was used as a binder compared to poly(ethylene propylene diene) (EPDM) and poly(tetrafluoroethylene) (PTFE). Li et al.[9] studied PTFE as a binder and suggested that PTFE decomposition might contribute to the irreversible capacity. Liu et al.[10] verified that the PTFE decomposed during the first discharge process and found that PVDF was more stable than PTFE. Nonfluorinated polymers such as EPDM[11,16] and copolymers such as vinylidene fluoride:hexafluoropropylene (VDF:HFP) and VDF:chlorotrifluoroethylene (VDF:CTFE) have also been examined,[16] with particular attention paid to the influence of the binder on the lithium/electrolyte reaction at the carbon surface and on heat generation.[15−17] From DSC experiments, Yamaki et al.[17] concluded that the surface covered by PVDF does not form the SEI at low temperature. Since the morphology and surface chemistry of polymeric binders affect the SEI formation and the irreversible capacity in various ways, it is important to understand the interface between binder and graphite; the ability to control it could lead to improved electrochemical performance.

In this paper, we examine PVDF binder interaction with graphite particles in slurries and final composite films. We selected PVDF because fluorinated binders have shown good reversible capacity and, among them, PVDF has emerged as the most promising because it provides electrochemical stability, reversibility, oxidation resistance, chemical resistance, and good wettability; moreover, it is available in large cost-effective quantities.[10,11,18] The PVDF binder/graphite interaction is first manifested in the viscosity of the high-solids-content slurry that is prepared prior to doctor blading into the final electrode film. Because such slurries are complex fluids with their rheological properties important for determining suspension stability, their study is closely related to the processing of composite electrodes. Our objectives are to describe the morphology and coverage of binder on the final composite anode and to correlate the graphite/binder interaction within the slurry with the surface properties of the final composite film.

Experimental Section

Composite Film Preparation. To investigate the effect of different surface area and type of carbon particles (amorphous or crystalline) on the interaction between carbon particles and PVDF, we used eight different carbon samples, which are listed in Table 1. Information on particle sizes and BET surface areas was obtained from the manufacturers. In most of our experiments, we used PVDF with a molecular weight of ≈350 000 (PVDF350, Kureha, KF1300), but we also examined a modified PVDF containing hydroxyl groups (PVDF350M, Atofina, MKB212A, M_w = ≈350 000) and a higher molecular weight PVDF (PVDF500, Atofina, Kynar301F, M_w = ≈500 000) for viscosity and adsorption experiments. The information on the molecular weights and head-to-head defects of PVDF is listed in Table 2. The slurry was prepared by mixing the carbon particles, 1-methyl-2-pyrrolidinone (NMP) (99.9+%, Mitsubishi Chemical Corp.) as a carrier, and 10 wt % solution of PVDF binder in NMP solvent. The compositional mix of carbon particles:PVDF:solvent in slurries was 38:2:60 wt %. We spread the slurry using the doctor-blade method on a sheet of copper foil and dried it in an oven at 83 °C in air for 2 h to form a 95/5 wt % graphite/PVDF composite anode with 34.5 (±0.5) μm thickness. To provide a reference sample, we deposited 5 wt % PVDF350/NMP solution on a cleaved, highly ordered pyrolytic graphite (HOPG) (10 × 10 × 1 mm, Structure Probe, SPI-2 grade) and dried it in the same way.

Slurry Characterization. Dynamic moduli and viscosities of the slurries were measured at 23 °C using a stress-controlled rheometer (DSR, Rheometric Scientific) for MPG-V2 and MBC-N and a strain-controlled rheometer (Dynamic analyzer RDA II, Rheometric Scientific) for the other samples. Two rheometers were required because the viscosities of MPG-V2

(12) DuPasquier, A.; Disma, F.; Bowmer, T.; Gozdz, A. S.; Amatucci, G.; Tarascon, J. M. *J. Electrochem. Soc.* **1998**, *145*, 472.
(13) Peled, E.; Menachem, C.; BarTow, D.; Melman, A. *J. Electrochem. Soc.* **1996**, *143*, L4.
(14) Hirasawa, K. A.; Nishioka, K.; Sato, T.; Yamaguchi, S.; Mori, S. *J. Power Sources* **1997**, *69*, 97.
(15) Maleki, H.; Deng, G. P.; KerzhnerHaller, I.; Anani, A.; Howard, J. N. *J. Electrochem. Soc.* **2000**, *147*, 4470.
(16) Richard, M. N.; Dahn, J. R. *J. Power Sources* **1999**, *83*, 71.
(17) Yamaki, J.; Takatsuji, H.; Kawamura, T.; Egashira, M. *Solid State Ionics* **2002**, *148*, 241.
(18) Barriere, B.; Miyaki, Y.; Despotopoulou, M.; Burchill, M. New PVDF binders for Li-ion batteries. Presented at the 10th International Meeting on Lithium Batteries (IMLB), Como, Italy, 2000.

Table 2. Functionality, Molecular Weight, and Head-to-Head Defects of PVDF Binder[a]

	manufacturer, product name	functionality	molecular weight	H−H defects (%) (from ^{19}F NMR)
PVDF350	Kureha, KF1300	N/A	≈350 000	4.22 (±0.53)
PVDF350M	Atofina, MKB212A	−OH (a little −COOH)	≈350 000	5.54 (±0.67)
PVDF500	Atofina, Kynar301F	N/A	≈500 000	6.55 (±1.24)

[a] The molecular weights of PVDF were provided by the manufacturers, and the head-to-head defects were calculated using ^{19}F NMR.

and MBC-N slurries were too low for the range of the strain-controlled rheometer. We used 40 wt % fixed solid concentration of slurries for all eight carbon samples, but we also examined 45 and 50 wt % solid concentration for the MPG-V2 and MBC-N samples. We used a 50-mm parallel plate with a 1-mm gap, and samples were prepared just before the experiments.

The storage and loss moduli are defined as[19]

$$\text{Storage (elastic) modulus: } G' = \tau'_o/\gamma_o \quad (1)$$

$$\text{Loss (viscous) modulus: } G'' = \tau''_o/\gamma_o \quad (2)$$

where τ'_o and τ''_o are the amplitudes of the stress when components are decomposed into two waves of the same frequency, one in phase with the strain and the other 90° out of phase, and γ_o is the strain amplitude. The complex viscosity is based on the storage and loss moduli, as follows:

$$\text{Complex viscosity: } |\eta^*| = (\eta'^2 + \eta''^2)^{1/2} = \left[\left(\frac{G''}{\omega}\right)^2 + \left(\frac{G'}{\omega}\right)^2\right]^{1/2} \quad (3)$$

where ω is the frequency in radians. η' is defined as the real component of the complex viscosity, and η'' is the imaginary component (elastic part) of the complex viscosity.

We varied the strain amplitude between 0.125% and 100% with a constant frequency of 1 rad·s^{-1} to determine the linear viscoelastic region, where rheological parameters are a function only of frequency. Next, we measured the storage and loss moduli and the complex viscosity as functions of the frequency in the range of 0.1−100 rad·s^{-1} at a strain amplitude of 0.4%.

Amount of Adsorbed PVDF. We measured the amount of adsorbed PVDF by centrifuging the slurries at 12 000 rpm (Avanti 30 centrifuge, Beckman) for 20 min at room temperature and separated the supernatant PVDF solution from the slurries containing adsorbed PVDF. Even though the NMP boiling point at atmospheric pressure (202 °C) is higher than the melting point of PVDF (160−175 °C measured by DSC), it can be lowered to 81−82 °C under a pressure of 10 mmHg. Therefore, we dried the polymer-adsorbed slurries at 95 °C in a vacuum for 48 h and then measured the amount of PVDF adsorbed on the graphite particles.

Morphology of PVDF on the Surface of Graphite. The spatial distribution of PVDF on the graphite particles was first evaluated with atomic force microscopy (AFM) and lateral force microscopy (LFM) on an MMAFM-2 (Digital Instruments) using a 125-μm piezoelectric scanner (5-μm z-height allowance). We used an oxide-sharpened Si_3N_4 cantilever with a sharp tip (200-μm length, 0.06 N/m spring constant, Digital Instruments NP-S). To study the PVDF distribution on the graphite particles, fluorine was mapped with electron probe X-ray microanalysis (EPMA) (JXA-733, JEOL) using 50 nA of current taken simultaneously with the secondary electron image, and then the degree of homogeneity was quantified.

Surface Coverage. The surface chemical composition of the graphite anodes was determined by X-ray photoelectron spectroscopy (XPS) (S-Probe, Surface Spectrometer) using a spectrometer equipped with an aluminum anode and a quartz monochromator that selected Al Kα X-ray radiation (1486.6 eV). The X-ray source was operated at 10 kV with a 35° electron takeoff angle from the sample surface. Survey scans (0−1000 eV) were performed first, followed by detailed scans of C_{1s}, O_{1s}, and F_{1s}. The spot size was 250 × 1000 μm for survey scans with 22 mA of current and 150 × 800 μm for detailed scans with 11 mA. Ion etching was performed at 10 μA current. For the sample of PVDF on HOPG, charge neutralization was achieved by an electron flood gun set at 1 eV.

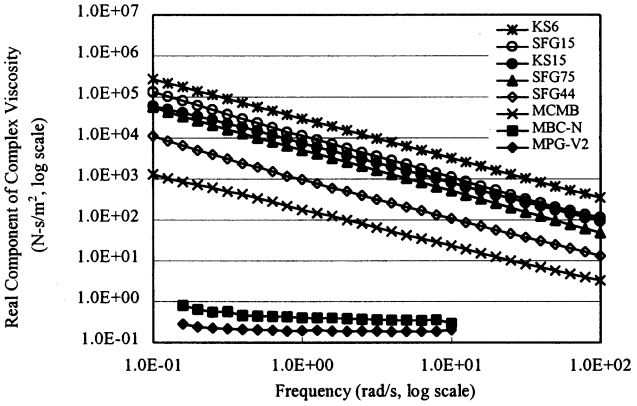

Figure 1. Dependence of the real component of complex viscosity on frequency for slurries containing different carbon particles, PVDF350, and NMP solvent at a strain amplitude of 0.4% at 23 °C. The concentration of particle:PVDF:solvent in slurries is 38:2:60 wt %. Viscosities range over 6 orders of magnitude with different carbon particles.

Results

Rheological Properties of Precursor Slurries. To investigate the interaction between graphite particles and PVDF in slurries before doctor-blading, we measured the slurry viscosities for a fixed solid concentration of 40 wt %, which is within the typical commercial range. Figure 1 shows the frequency dependence of the real component of complex viscosity, which ranges over 6 orders of magnitude for different carbon particles. For MPG-V2 and MBC-N, the real components of complex viscosity are nearly independent of frequency on a log−log scale with power law dependence ($\eta \propto \omega^{n-1}$) on a frequency of $n = 0.997$ and 0.974, respectively, which indicates that these behave as Newtonian interfaces. On the other hand, the viscosities of the other slurries decrease linearly as frequency increases with a power between $n = 0.165$ for MCMB and $n = 0.038$ for KS6. This shear thinning is typical non-Newtonian behavior, which is found in many colloidal suspensions and polymer solutions.[19] In concentrated particle/polymer suspensions such as these, a three-dimensional network is developed due to bridging flocculation[20] and/or the attractive interaction between adsorbed polymer layers. In such suspensions, structural breakdown is induced with increasing shear rate, leading to shear thinning.

(19) Macosko, C. W. *Rheology: Principles, Measurements and Applications*; VCH: New York, 1994.

(20) Healy, T. W. *J. Colloid Sci.* **1961**, *16*, 609.

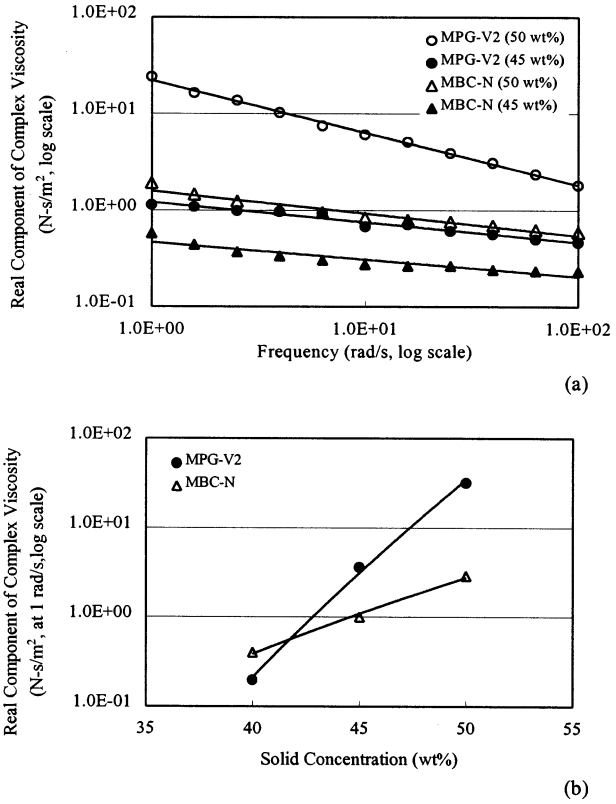

Figure 2. (a) Dependence of the real component of complex viscosity on the frequency and (b) the real component of complex viscosity at 1 rad/s in terms of solid concentration for MPG-V2 and MBC-N with PVDF350. As the solid concentration increases, the viscosity increases and the slurries show shear-thinning behavior.

This behavior is desirable for processing[21] because the slurry viscosity decreases under the shear stresses generated by the doctor blade but returns to a high level after the shear is released.

We were not able to make slurries of higher concentration for all carbon samples since some of them already exhibit very high viscosity with 40 wt % solid concentration. However, to relate the rheological behavior of the low-viscosity MPG-V2 and MBC-N samples, which exhibit Newtonian behavior at 40 wt %, to the others, we also examined higher solid concentrations of 45 and 50 wt %, with the results shown in Figure 2. In contrast to the behavior for the 40 wt % slurry, these higher concentration slurries show weak shear thinning behavior with a power between $n = 0.46$ for MPG-V2 (50 wt %) and $n = 0.91$ for MBC-N (45 wt %), as shown in Figure 2a. These values are much higher than those of the other samples that show shear-thinning behavior in Figure 1, which results from the apparently weak interaction of MPG-V2 and MBC-N with PVDF. Figure 2b shows that as the solid concentration increases from 40 to 50 wt %, the viscosity increases significantly for MBC-N and MPG-V2. This demonstrates that the interaction between carbon particles and PVDF increases due to more adsorption sites for PVDF in the presence of more particles. The MPG-V2 sample appears to be more sensitive to the solid concentration than MBC-N. The Newtonian behavior and the low viscosities

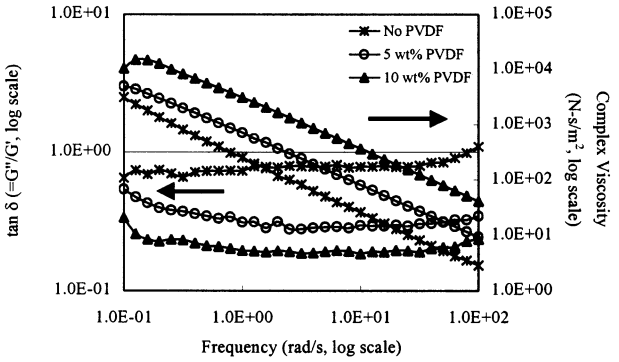

Figure 3. Effect of PVDF concentration on the interaction between PVDF and graphite particles. PVDF350 and MCMB were used and the data were taken at a strain amplitude of 0.4%. The overall solid concentration is 40 wt % and the PVDF concentration in the slurries varies.

of these two samples at 40 wt % solid concentration in Figure 1 are presumably due to weak interaction between graphite particles and PVDF.

The effect of PVDF concentration was investigated for 40% total solid concentration but different PVDF concentration in the solids content, as illustrated in Figure 3. As the PVDF concentration increases, the viscosity increases, and tan δ, which is defined as loss modulus divided by storage modulus, decreases, indicating that the addition of PVDF to graphite makes the slurries more elastic. This suggests that a more well-developed network is generated by a larger amount of the polymeric binder. Shear thinning occurs in all the samples for high frequency. The increase in viscosity upon addition of polymer has been found in many other slurry systems containing high molecular weight polymers.[22,23] Also, Kiratzis and Luckham[22] showed that the storage modulus increases as the polymer volume fraction or solids volume fraction increases.

To verify that the increased viscosity results from the interaction between particles and polymer, we used a PVDF sample modified by functionalization with hydroxyl groups and a higher molecular weight PVDF for the viscosity measurements, with the result shown in Figure 4. The graphs illustrate the frequency dependence of slurry viscosities containing PVDF350, PVDF350M, and PVDF500 with MCMB or SFG44 graphite materials. These two graphite samples were chosen due to similar BET surface areas and viscosities. The effect of PVDF chemical properties is not large because the PVDF content is merely 2 wt % in the slurries. Nevertheless, we note that the higher molecular weight PVDF (PVDF500) and the PVDF modified with hydroxyl groups (PVDF350M) show higher viscosities compared to PVDF350. The PVDF500 caused the viscosities to be increased because high molecular weight polymer can adsorb more to the particles and bridge particles together with longer chains, leading to a more flocculated network structure. PVDF350M increases the viscosity of slurries through the enhanced hydrogen-bonding capability of the hydroxyl functionalization, leading to increased adsorption and a higher viscosity. PVDF500 and PVDF350M show almost the

(21) Pagnoux, C.; Chartier, T.; Granja, M. D.; Doreau, F.; Ferreira, J. M.; Baumard, J. F. *J. Eur. Ceram. Soc.* **1998**, *18*, 241.

(22) Kiratzis, N. E.; Luckham, P. F. *J. Eur. Ceram. Soc.* **1999**, *19*, 2605.

(23) Otsubo, Y. *Chem. Eng. Sci.* **2001**, *56*, 2939.

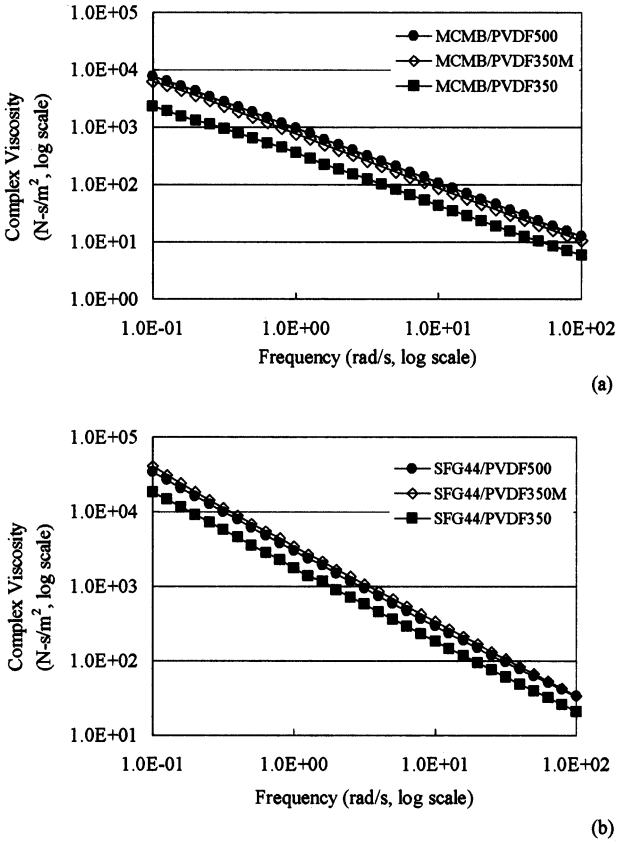

Figure 4. Complex viscosity of (a) MCMB and (b) SFG44 graphite influenced by the chemical properties of PVDF at a strain amplitude of 0.4%. The concentration of particle:PVDF: solvent in slurries is 38:2:60 wt %.

same viscosity for each graphite material, which means that the interaction due to hydrogen bonding is equivalent to that of high molecular weight.

To isolate the effect on the viscosity (Figure 4) due to the interaction between graphite particles and PVDF, we separately measured the polymer solution viscosity in NMP. The viscosities of 10 wt % PVDF solution at a frequency of 1 rad/s are 0.491, 0.395, and 1.184 Ns/m^2 for PVDF350, PVDF350M, and PVDF500, respectively. PVDF500 shows the highest viscosity due to the higher molecular weight, and PVDF350M shows the lowest viscosity, presumably due to a reduced hydrophobic interaction between polymer and NMP. Note that the slurry viscosity with PVDF350M is comparable to that of PVDF500 even though pure PVDF500 solution shows a higher viscosity than does pure PVDF350M. Because the amount of PVDF in the slurries is small, it is difficult to separate the effect of PVDF molecular weight from the rheological properties. Nevertheless, this result certainly indicates that the presence of the hydroxyl functional group is the source of enhanced interaction with the graphite particles, leading to a more extensive network structure of the suspension and, consequently, a higher viscosity.

Since the slurry viscosity results reflect the interaction between particles and polymer, it should be possible to relate the amount of adsorbed polymer to the viscosity. To address this, we carried out centrifuge experiments to find out how much polymer is adsorbed onto the surface of the graphite particles. We assumed that the centrifugal force is sufficient for separating unadsorbed polymer from the adsorbed polymer and that there is no confined PVDF due to solvent being trapped inside the graphite particles. Figure 5 shows the relationship between the percentage of adsorbed PVDF and the complex viscosities of slurries of Figure 4, illustrating that an increase in adsorbed polymer leads to a higher viscosity. This suggests that the interaction between particles and PVDF results from the bridging interaction of loops and tails of polymer segment with other graphite particles and/or the interaction between adsorbed polymer layers.

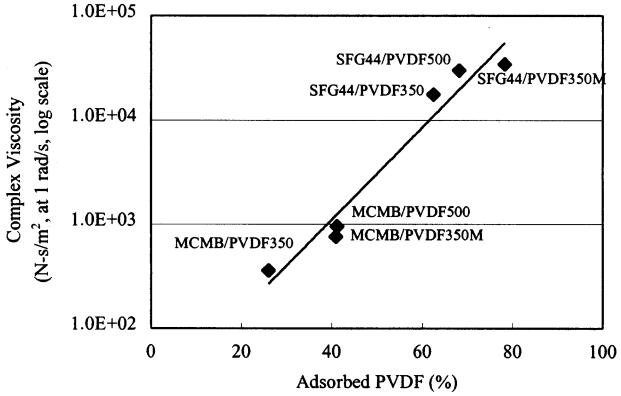

Figure 5. Dependence of complex viscosity on the percentage of PVDF adsorbed on the graphite particles. The increase of viscosity with an increase in the percentage of adsorbed PVDF is due to the interaction between adsorbed polymer layers and/or bridging interaction.

Morphology of PVDF. The morphology of PVDF on the surface of graphite or carbon in composite films was studied using AFM, LFM, and EPMA. A $1 \times 1\ \mu$m image of contact mode AFM shown in Figure 6a exhibits the topography of the SFG15 sample. This image shows graphite grain boundaries, but we cannot distinguish the polymeric binder from the graphite. By contrast, LFM identifies and maps relative differences in surface frictional characteristics by detecting the lateral bending of the cantilever. Since graphite and PVDF are expected to have different frictional forces, LFM can be an effective tool for distinguishing the PVDF region from the graphite surface. Parts b and c of Figure 6 show trace and retrace LFM images, respectively, taken simultaneously with the AFM image for a rotation value of +90°. In Figure 6b, the darker area corresponds to a low-friction region that is bare graphite, while the lighter area indicates the higher friction of binder-covered regions.[14] In the retrace LFM image of Figure 6c, the image contrast is reversed because the lateral twisting direction of the cantilever is altered with respect to the scanning direction; here, the darker area corresponds to the PVDF binder region. To obtain a more accurate image, we subtracted the retrace LFM image from the trace LFM image, resulting in an image with a friction force twice that of the trace image and having diminished errors in LFM images, as expected. This image is shown in Figure 6d, where the darker area indicates the graphite region. In LFM images, we can observe the edge surface of graphite with the thickness of about 0.5 μm, which is in good agreement with reported data.[5] Also, we observe the layered structure of graphite, which is not apparent in the AFM image, and we can distinguish the polymer-coated region from

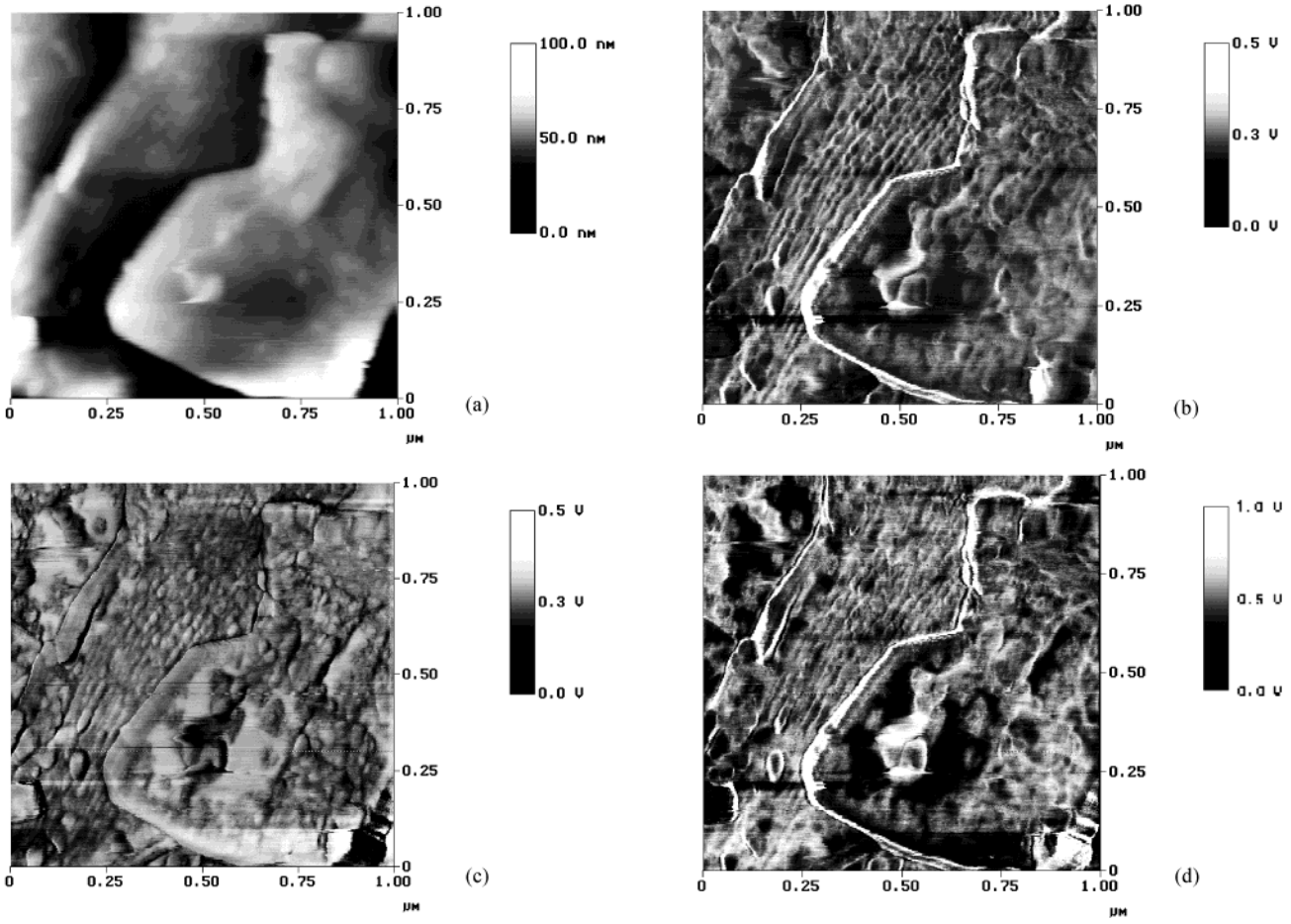

Figure 6. AFM and LFM images of the SFG15 sample. (a) AFM image, (b) a trace LFM image, (c) a retrace LFM image, and (d) trace minus retrace image, indicating PVDF shows inhomogeneous distribution on the surface of graphite particles.

the bare graphite region because of the different friction forces.

From the LFM images, we observe that the PVDF is inhomogeneously distributed on the graphite surface. In all the images, the polymeric binder appears to cover the surface at levels lower than the 70% reported by Hirasawa et al.[14] This difference may result from the small size (1×1 μm) of the AFM and LFM images, which permits only a localized value of the PVDF coverage to be determined. Nevertheless, it appears quite clear that PVDF shows preferential deposition on the edges of the graphite particles; this was verified with EPMA data, as described in the following.

EPMA can identify an element through use of a crystal monochromator to select X-rays of a particular wavelength. With a repeating unit of $-(CH_2-CF_2)-$, the location and morphology of PVDF on the carbon can be easily observed by monitoring fluorine with EPMA. Since the depth of field of EPMA is about 1 μm, we cannot detect the *exact* surface morphology of PVDF, but rather we determine a *near*-surface morphology. Figure 7a shows a secondary electron image of MBC-N carbon taken by EPMA with a magnification of 1000. We scanned 500 times to detect fluorine, which is shown as relatively nonuniform distribution in Figure 7b. When we superimposed this picture upon Figure 7a, we determined that PVDF is preferentially located at the edges and grain boundaries of the carbon particles, as shown in Figure 7c. Figure 7d is a magnified image of one region of Figure 7c, which more clearly shows a heterogeneous distribution and aggregated PVDF on the particle edges. This phenomenon is attributed to the fact that the polar polymer prefers polar surfaces such as the edges of carbon, which contain many dangling bonds and surface oxygen.[24]

Figure 8a–f shows fluorine dot mappings of the composite films with different carbon materials. When these images are superimposed on the secondary images of the respective carbon or graphite particles, fluorine again appears to be mainly located on the edges and grain boundaries, as was shown in Figure 7 for MBC-N. These images are listed in the order of increasing slurry viscosity (see Figure 1), illustrating that the distribution of PVDF in the final composite film becomes more homogeneous with increasing viscosity. To minimize the influence of carbon particle size on the images of apparent polymer distribution, we used different magnifications at which all the graphite samples have approximately the same size.

In an attempt to semiquantitatively assess the degree of homogeneity, we developed a simple, geometric approach. In this method, we drew many random lines across the fluorine maps and used Scion Image software to determine the distances between the fluorine dots that happened to be intersected by those lines. Follow-

(24) Nakajima, T.; Koh, M.; Singh, R. N.; Shimada, M. *Electrochim. Acta* **1999**, *44*, 2879.

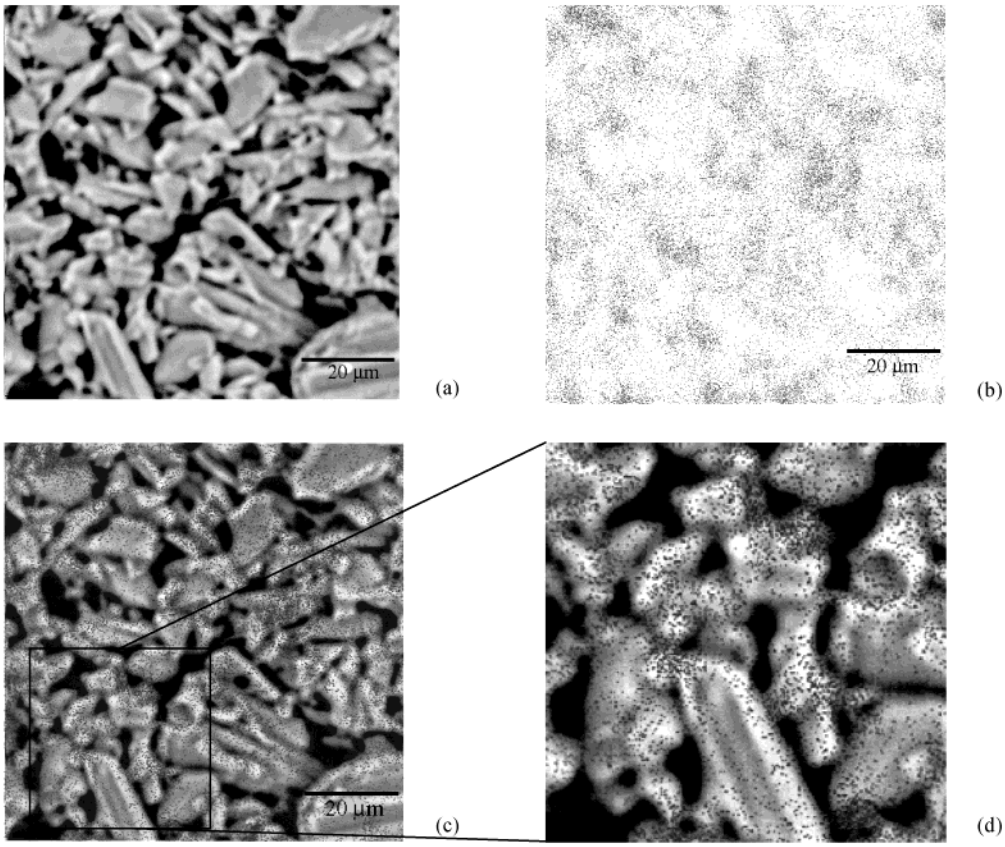

Figure 7. EPMA images of MBC-N. (a) shows the carbon particles and (b) shows fluorine dot mapping, indicating inhomogeneous PVDF distribution. (c) is a superimposed image illustrating that PVDF is preferentially located on the edges and grain boundaries of carbon. (d) is a detail of one region of (c).

ing this, we determined the distribution of the dot-to-dot distances and calculated their standard deviations. In this way, we were able to relate the standard deviation to the degree of homogeneity. For samples in which the distribution of PVDF is inhomogeneous, the distances between fluorine dots will vary considerably, leading to a large standard deviation. On the other hand, if the PVDF distribution is homogeneous, the distances will show a narrow distribution, leading to a small standard deviation. To establish reproducibility, we drew at least 10 lines, each containing around 500 dots. The standard deviation is plotted versus the real component of complex viscosity at 1 rad/s of frequency on a log scale in Figure 9, which shows a clear linear relationship. Samples with low viscosity show a larger standard deviation, indicating less homogeneous distribution of PVDF. The good correlation with this rather simple data analysis suggests that it is a useful empirical technique.

This distribution analysis result was verified by a more sophisticated approach using the autocorrelation function, $C(R)$, which describes the spatial correlation of the density of dots in an image and is defined as the average normalized by $C(0)$,[25]

$$C(R) = \frac{\langle[\rho(r) - \rho_o][\rho(r - R) - \rho_o]\rangle}{C(0)} \qquad (4)$$

where ρ is the dot density distribution and the angular brackets indicate averaging over all coordinates r. When r is equal to 0, there is a strong self-correlation peak corresponding to each image correlating with itself. When r is equal to the mean displacement, there is a second peak called a positive displacement peak, which corresponds to the first image correlating with the second image. From this characteristic of the autocorrelation function, we can calculate the area of a cluster and the spacing between clusters. Each image was normalized so that its maximum is unity, and radial averaging was performed to transform the two-dimensional image to the one-dimensional spatial peak shown in Figure 10a. The area under the first peak corresponds to the size of a cluster and the distance to the second peak indicates the radial average spacing between two clusters. We plotted the spacing versus the normalized area of clusters of each sample in Figure 10b; small cluster size and reduced distance between clusters of dots denote homogeneous distribution. While MBC-N shows the largest cluster area and radial spacing, indicating an inhomogeneous PVDF distribution, KS6 exhibits the smallest area and spacing, indicating the most homogeneous distribution. Figure 10c shows the relationship between the degree of homogeneity and the viscosity derived from the autocorrelation method, which is consistent with the result in Figure 9. The autocorrelation method depends more on the sample size and the magnification than the standard deviation method. Therefore, there may be an influence of the distribution of particle size on the spacing and area of peaks from the autocorrelation. Nonetheless, from these

(25) Strobl, G. R.; Schneider, M. *J. Polym. Sci., Part B: Polym. Phys.* **1980**, *18*, 1343.

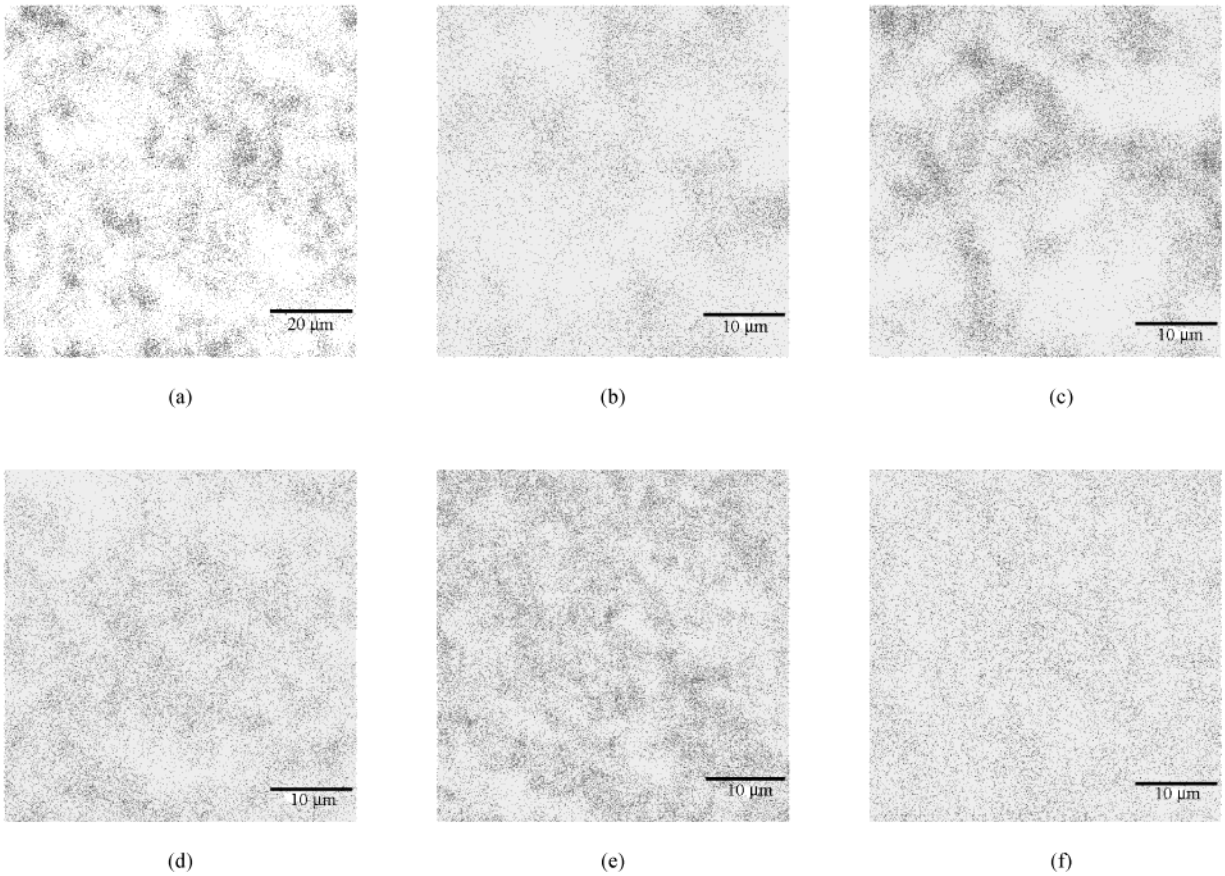

Figure 8. Fluorine dot mapping of (a) MBC-N (average particle size of 18 μm), (b) MCMB (7.8 μm), (c) SFG44 (22 μm), (d) KS15 (7.7 μm), (e) SFG15 (8.1 μm), and (f) KS6 (3.3 μm). These images are shown in the order of increasing viscosity. 120 pixels corresponds to 20 μm for (a) and 10 μm for (b), (c), (d), and (f). For (e), 116 pixels corresponds to 10 μm.

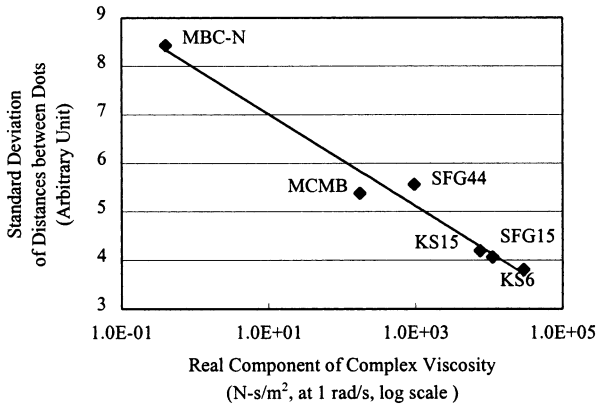

Figure 9. Correlation of standard deviation of distances between fluorine dots with the real component of complex viscosity. The scale of standard deviation is arbitrary.

data we are able to relate the viscosity to the surface properties of the final films.

Surface Coverage. The surface chemistry was investigated using XPS. Table 3 shows the atomic fraction (%) of carbon, fluorine, and oxygen. In the PVDF-on-HOPG sample, we found that the ratio of fluorine to carbon is about 1, which is expected, and does not contain any oxygen. In graphite samples, however, a significant amount of oxygen is detected, which results from surface-oxygenated species such as carbonyl, carboxyl, and hydroxyl groups in the surface edge planes of the graphite particles.[24] The amount of the surface oxygen increases as the crystallinity decreases,[24] which is demonstrated by the large atomic fraction for the amorphous MBC-N sample. Also, MBC-N shows around 3−10% more fluorine before etching and twice more after etching than do the other samples. This is due to the fact that amorphous carbon is randomly and loosely packed with a large number of dangling bonds, which leads to an increase in the amount of oxygen and fluorine at the surface. These surface sites are important for the surface chemical composition because polymeric binders may be adsorbed onto nanopores or dangling bonds in the amorphous carbon. After being etched for 1 min with an Ar ion gun, resulting in about 120 Å etching, the fraction of fluorine significantly decreases, indicating that PVDF binders exist much more at the surface of the graphite. Surface oxygen is completely eliminated after etching.

Table 3 shows that the fraction of fluorine is at a maximum value of 0.20 in the case of amorphous carbon. Since the mean free path of an electron is about 18 Å, if the polymer layer is thicker than 18 Å, we cannot detect the graphite substrate. In this case, because the carbon:fluorine ratio with the PVDF layer is 1:1, the total atomic fraction from the PVDF layer will be 0.4 with the fluorine fraction of 0.2, indicating that 40% of the graphite surface is covered by PVDF. On the other hand, if the PVDF thickness is less than the mean free path of an electron, XPS can detect the graphite underlying the PVDF, which makes PVDF coverage calculation more complicated. To investigate the coverage of polymer on the surface of graphite by XPS, we

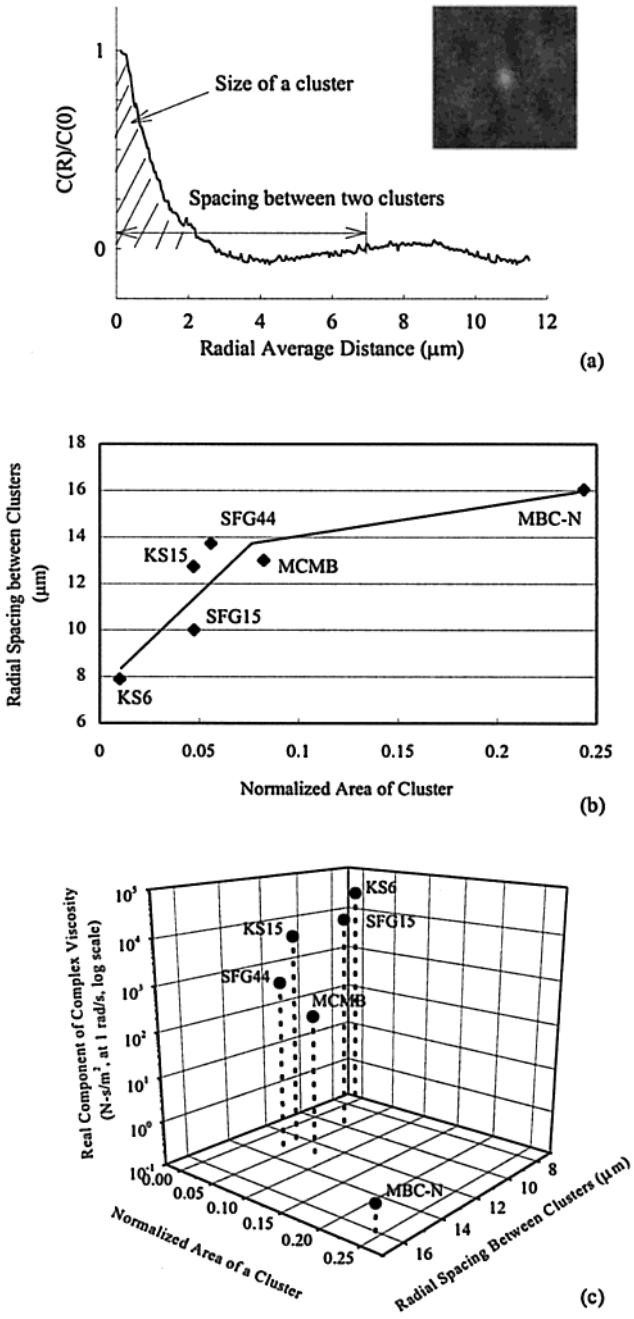

Figure 10. (a) 1-D radial averaged autocorrelation normalized by *C*(0), which is transformed from a 2-D autocorrelation image shown as an inset. The area of the first peak indicates the size of a cluster, and the distance to the second peak corresponds to the radial average spacing between two clusters. (b) Plot of radial spacing between clusters in terms of normalized area of cluster measured by the autocorrelation function. The homogeneity of PVDF distribution increases as the spacing between clusters and the area of a cluster decrease. (c) 3-D graph showing the relationship between the degree of homogeneity and the real component of complex viscosity.

etched the surface of the SFG15 film with an Ar ion gun in increments of 2-Å thickness and then measured the atomic composition. The fraction of fluorine decreased exponentially with etching, and only a small amount of fluorine existed after etching for a long time, as shown in Figure 11. The 5-Å-etched film showed that about half of the fluorine content is left, and from that point, the rate of decrease in fluorine content is apparently

Table 3. Atom Fraction (%) of Carbon, Fluorine, and Oxygen in Each Sample[a]

	relative percentage (%)		
sample	C	F	O
PVDF on HOPG	48.91	51.09	0
MPG-V2	81.03 (97.63)	17.33 (2.37)	1.64 (0)
MBC-N	75.62 (95.44)	20.09 (4.56)	4.29 (0)
MCMB	87.65 (97.25)	9.84 (2.75)	2.51 (0)
SFG15	83.48 (97.69)	13.99 (2.31)	2.53 (0)

[a] The values in parentheses are obtained after Ar ion etching of 120 Å.

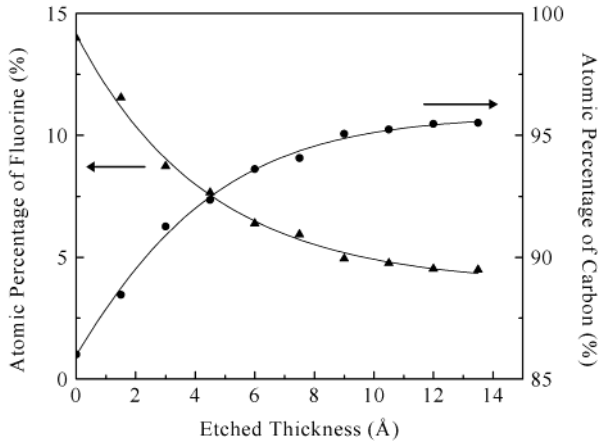

Figure 11. Depth profile of the SFG15 composite film. We measured the atomic percentage of carbon and fluorine after each etching. Around 5-Å etching causes half of the fluorine to be left.

reduced. The surface coverage based on these data is considered further in the Discussion section.

Discussion

Interaction between Particles and PVDF in Slurries. In concentrated suspensions, it is generally believed that the rheological behavior is affected by particle size, size distribution, solid concentration, and interparticle forces.[26,27] As the particle volume fraction increases and the particle size decreases, the viscosity and the shear yield stress significantly increase.[26,27] In this paper, we used the same weight concentration for all the samples; therefore, we can exclude the effect of the particle volume fraction on the rheological properties if we apply the theoretical bulk density of graphite (2.26 g/cm^3), which does not consider closed porosity. Particle size and size distribution will, however, affect the packing density of the particles and the microstructure of the suspension.[26] The packing fraction of samples having small particle size is high, and these samples have a compact structure with less space between the particles, leading to high viscosity. Moreover, if particles are small, solvent molecules introduced can be trapped in the voids of the graphite particles.[27] The solvent cannot easily move between particles, and internal friction increases, causing an increase in the viscosity of the slurry. However, as shown in Table 1, we observed that the particle sizes are not directly related to their viscosities. While KS6, which has the smallest particle

(26) Zhou, Z. W.; Scales, P. J.; Boger, D. V. *Chem. Eng. Sci.* **2001**, *56*, 2901.
(27) Yavuz, R.; Kucukbayrak, S. *Energy Sources* **1998**, *20*, 787.

size (3.3 μm), shows the highest viscosity, SFG75, with the largest particle size (27 μm), and SFG44 (22 μm) also show much higher viscosity than do MPG-V2, MBC-N, or MCMB, which have somewhat smaller particle sizes (18.4, 18, and 7.8 μm, respectively). In addition, if the particle size distribution in the suspension is broad, small particles can easily be introduced into the void spaces of the coarser particles[26,27] with dense structures being formed, thus leading to high viscosity. SFG44 and SFG75 have a broader particle size distribution (2−128 μm) than other samples (1−8 μm for KS6 and 2−48 μm for KS15 and SFG15), which can contribute to their high viscosities despite large particle sizes.

However, with the packing geometry resulting from the physical properties of graphite, for example, the size and size distribution of particles, we cannot explain all the rheological properties. This is due to the fact that the physical properties can influence the surface area, leading to an effect on reactive sites of graphite, which influence the interaction mechanism of polymer with graphite. Comparing the BET surface areas among carbon materials in Table 1, we observe that samples with low BET surface area (MPG-V2, MBC-N, MCMB, SFG44, and SFG75) generally show lower viscosity than KS15, SFG15, and KS6, which have high BET surface area. High surface area can lead to extensive interaction between graphite and PVDF through greater adsorption area, even though the ratio of edge plane to basal plane in the surface area would also be important for determining the *interacting* sites with PVDF.

The influence of reactive sites on the interaction can be examined by using a modified PVDF. When we used a PVDF sample modified by −OH functional groups (PVDF350M) with the same molecular weight as that of PVDF350, the dynamic viscosity increased for the same graphite, as shown in Figure 4. This indicates that the altered interaction between graphite and PVDF through the hydroxyl functional group leads to different slurry microstructures. Therefore, the different viscosities do not originate solely from the physical characteristics of the graphite particles, and we need to consider particle−particle interactions as well as those between particle and polymer.

The van der Waals attraction, which is due primarily to the interaction of instantaneous dipoles generated within the atoms, is the major force responsible for an interconnected network of substantial mechanical strength when there are no repulsive forces between the particles. At low shear rates, the suspension structure is close to equilibrium since thermal motion dominates over the viscous forces. At higher shear rates, the viscous forces affect the suspension structure more, causing the structure to become distorted, hence leading to shear thinning. It has been demonstrated that a concentrated suspension becomes more severely shear thinning with an increase in the magnitude of the interparticle attraction.[28] Samples with high surface area can generate such high interparticle interaction. Therefore, KS15, SFG15, and KS6 show higher viscosity than the others even in the absence of PVDF. However, in our concentrated slurry system, we also need to consider the role of PVDF in the interaction of graphite particles.

PVDF can form hydrogen bonds[29,30] between its fluorine atoms and hydrogen from graphite. As a result, it is able to physisorb to the surfaces of graphite, especially on the edges containing H atoms. Hydrogen bonding exists when hydrogen is joined to an electronegative element such as fluorine, oxygen, or nitrogen by a covalent bond, which leads to electrons distributed so unevenly that the exposed proton at the hydrogen end is strongly attracted to nonbonding pairs of electrons on other molecules. In the XPS experiments, we found no correlation between the oxygen content and the viscosity. Therefore, we presume that hydrogen bonding between graphite and PVDF results from the bonding between hydrogen atoms in graphite and fluorine atoms in PVDF rather than between the surface oxygen on graphite particles and the hydrogen atom in PVDF. Such hydrogen bonding is well-established, but weak.[31] Moreover, the polymer cannot be completely confined to the surface, and a significant fraction of the adsorbed polymer projects away from the surface as loops and tails.[32] Surfaces interact with each other through these loops and tails, and the range of interaction prescribes the overall thickness of the adsorbed layers. If the surfaces are completely covered with adsorbed polymer, the osmotic pressure of polymer segments between particles generates a repulsion, which leads to depletion stability. On the other hand, a high molecular weight polymer with low surface coverage, usually at half-surface coverage, can hold particles together by bridging two or more particles, leading to aggregated macroscopic structures.[20,33] In our system, high molecular weight PVDF was used at a low concentration (2 wt % in slurries), and AFM/LFM and XPS data suggested that the polymer does not cover the whole surface of graphite, but forms discrete polymer domains. Therefore, PVDF seems to be adsorbed onto the surfaces of graphite through hydrogen bonding and physisorption, such that loops and tails can interact with other particles and/or another adsorbed polymer layer, leading to aggregated particles with high viscosity. Figure 5 supports the conclusion that the viscosity reflects the interaction between polymer and particles.

PVDF Distribution in Films. We have established that the degree of homogeneity of PVDF distribution on the composite film is proportional to the precursor slurry viscosity. This result allows us to relate bulk properties before processing to the distribution of binders after doctor-blading a composite anode, followed by curing. Samples that retain high viscosity show a more homogeneous distribution of PVDF than low-viscosity samples. This is attributed to the fact that large particles, which generally show low viscosity, have small surface areas and, therefore, relatively small interacting sites with PVDF. This generates a weak interaction between graphite and the polymer, leading to aggrega-

(28) Woutersen, A.; Dekruif, C. G. *J. Chem. Phys.* **1991**, *94*, 5739.
(29) Yano, S.; Iwata, K.; Kurita, K. *Mater. Sci. Eng. C* **1998**, *6*, 75.
(30) Biswas, A.; Gupta, R.; Kumar, N.; Avasthi, D. K.; Singh, J. P.; Lotha, S.; Fink, D.; Paul, S. N.; Bose, S. K. *Appl. Phys. Lett.* **2001**, *78*, 4136.
(31) Desiraju, G. R.; Steiner, T. *The Weak Hydrogen Bond in Structural Chemistry and Biology*; Oxford University Press: Oxford; New York, 1999.
(32) Stuart, M. A. C.; Waajen, F.; Cosgrove, T.; Vincent, B.; Crowley, T. L. *Macromolecules* **1984**, *17*, 1825.
(33) Lafuma, F.; Wong, K.; Cabane, B. *J. Colloid Interface Sci.* **1991**, *143*, 9.

Table 4. Percentage of Fluorine Density in the Edge Part of Carbon Particles. around 50% of PVDF Resides at the Edge Part of Graphite and This Amount Decreases as Viscosity Increases

	MBC-N	SFG44	SFG15
fluorine density at edges (%)	53.2 (±0.3)	51.8 (±0.3)	49.6 (±0.4)

tion of PVDF instead of the homogeneous distribution. On the other hand, small particles having large surface interacting sites with PVDF show increased interaction with the polymer, leading to a more homogeneous distribution.

LFM and EPMA data have shown the preferential distribution of PVDF on the edges and the grain boundaries of the carbon particles. This is attributed to the fact that polar polymer prefers the polar surface. In addition, we can also consider the entropy penalty. Polymer adsorption occurs when the enthalpic component of attractive polymer−surface compensates the configurational and conformational entropy loss of polymer, which results from confinement to the surface. The entropy penalty is less for adsorption on a rough surface with the roughness being on the scale of the polymer dimensions, which has been studied with carbon black and carbon fiber filled polymer blends.[34] There it was shown that the polymer preferentially adsorbs at the rough ends of carbon filaments and on the edge surfaces of carbon crystalline particles.[34] We estimated how much PVDF resides on the edge part of carbon particles by calculating the ratio of density of dots within 0.8 μm [Due to picture resolution, we were not able to use smaller thickness] of carbon edges to that inside the particle excluding the edge part using the EPMA images. The result is shown in Table 4, indicating that around 50% of the PVDF binder is concentrated on the edge part of carbon particle, with the remaining 50% PVDF being distributed all over the particle. The percentage of fluorine density in the edge part of graphite decreases somewhat as the viscosity of the slurry increases. However, the difference is small in contrast to the variation in the degree of homogeneity of PVDF distribution (Figures 9 and 10). This is probably due to the similar reactivity and roughness of edge parts of all the graphite particles and the error in defining the edge part of carbon particles.

Surface Coverage Model. The etching data (Figure 11) are interpreted in terms of two schemes, as shown in Figure 12. First, some of the graphite surface may be covered by 5-Å-thick PVDF before etching, while the other half may be covered by thick films (more than an electron mean free path) (Figure 12a). Second, if there are only thick PVDF aggregates on the graphite surface, as shown in Figure 12b, we suggest that a concentration gradient in the PVDF aggregates could exist, which can lead to less fluorine with the 5-Å etching. If we assume the former scheme to apply and a uniform film with an electron mean free path of 18 Å, we can detect 5/18 atoms from the 5-Å-thick layer and half of them would be fluorine (carbon:fluorine = 1:1 in PVDF); therefore, we detect 5/36 of fluorine ratio to total atoms ((5/18) × (1/2) = (5/36)) from the 5-Å-thick layer. From the thicker aggregated PVDF, we detect half fluorine atomic ratio. A simple calculation with this two-region model gives a 0.3% graphite region thickly covered by PVDF and 99.7% by the 5-Å-thick layer. From those values, we are not able to obtain the fluorine fraction of 0.07 after 5-Å etching, as shown in Figure 11. Therefore, we support the second scheme with discrete PVDF regions on the surface of graphite particles.

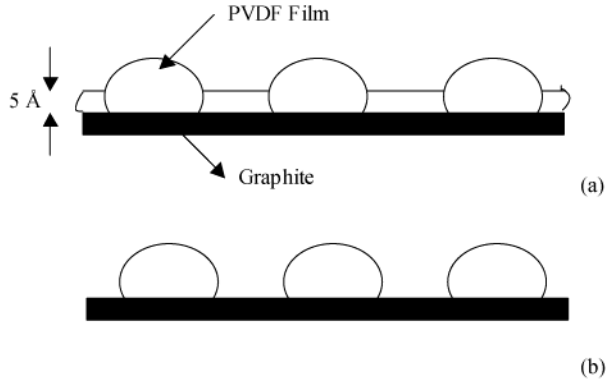

Figure 12. Schemes for the surface coverage of PVDF on the graphite. (a) shows some aggregated PVDF with 5-Å films in other regions. (b) indicates discrete aggregates of PVDF. It is assumed that graphite particles have a negligible thickness fluctuation and are flat. Not scaled.

There is additional evidence that supports the second scheme. First, bridging flocculation tends to occur when the polymer coverage is at about 50%,[33] while depletion flocculation occurs if the surface is saturated. If we assume that there is 5-Å-thick film covering the entire region except for the thickly covered region, the polymer coverage is unity, and bridging flocculation may not occur. Second, LFM data show a bare graphite surface, which suggests that there is a region not covered by a 5-Å-thick film. Therefore, the results support the second model in which the polymer covers a maximum of 40% of the graphite surface with discrete aggregate morphology of PVDF. There may be an error for this coverage because the basic assumption of these schemes is the uniform and flat surface of graphite, which is unfortunately not a real case. However, this method can provide an estimated coverage by assuming that the surface thickness fluctuation of the graphite is much smaller than the spot size of XPS, which can be overcome somewhat by using SFG15, which has a rather flat surface.

Summary

In this paper, we have demonstrated that different graphite samples show a large range of slurry viscosity caused not only by the physical properties of graphite particles but also, more importantly, by the interaction between graphite and PVDF. Adsorbed polymer interacts with other particles and/or other polymer layers, leading to aggregated structures and high viscosity. When we used the hydroxyl-modified PVDF, the adsorption of polymer and the flocculation of graphite particles are enhanced through improved hydrogen-bonding capability of the modified PVDF. This particle/polymer interaction in slurries affects the final morphology of PVDF on graphite. PVDF shows more

(34) Wu, G. Z.; Asai, S.; Sumita, M.; Yui, H. *Macromolecules* **2002**, *35*, 945.

homogeneous distribution in high-viscosity samples and is preferentially located at the edges or grain boundaries of graphite. XPS data show that the carbon structure is related to the coverage of PVDF, and a maximum of 40% of the graphite surface is thickly covered by PVDF with the discrete aggregate morphology of PVDF. This study of particle/PVDF interaction is important in understanding and controlling the final film properties influenced by the processing parameters such as viscosity, which would contribute to the improvement of the electrochemical efficiency in lithium ion batteries.

Acknowledgment. This work was supported by Mitsubishi Chemical Corporation. We acknowledge valuable discussions with Professor Bruce M. Clemens for the autocorrelation function. Also the authors thank Bob Jones for collecting the EPMA data.

CM0209970